PAPER

Check for updates

Interfacial engineering by creating Cu-based ternary heterostructures on C_3N_4 tubes towards enhanced photocatalytic oxidative coupling of benzylamines†

Yunqi Fu,[a] Mang Zheng,[a] Qi Li,[a] Liping Zhang, [ID] *[b] Shuai Wang,*[c] V. V. Kondratiev[d] and Baojiang Jiang [ID] *[a]

Benzylamine coupling is a very important reaction for the synthesis of imine but still faces many challenges. Herein, we present a highly effective strategy towards the coupling reaction by using environmentally friendly catalysts. These catalysts are composed of $Cu/Cu_2O/Cu_3N$ heterostructures supported by C_3N_4 tubes and the composites were synthesized by one-step hydrothermal treatment followed by calcination. Cu_2O, Cu_3N, and C_3N_4 all are responsive to visible light and the heterojunction formed can greatly enhance the charge separation. When used as photocatalysts for oxidative self-coupling of benzylamine at a low temperature of 323 K in air, $Cu/Cu_2O/Cu_3N/C_3N_4$ was able to give conversion and selectivity values of up to 99% and 98%, respectively. The high efficiency of the catalysts is attributable to their ability to generate large quantities of free radicals (such as $\cdot OH$ and $\cdot O_2^-$) under visible-light irradiation.

1. Introduction

Imines are important intermediates in the synthesis of many organic compounds.[1,2] The traditional synthetic method for imines is the condensation of amines with carbonyl compounds, which generally needs costly dehydrating agents, and Lewis acids as the catalysts.[3,4] However, this method is not only cumbersome to operate, but also causes some side reactions, and even causes serious pollution to the environment. Alternatively, the direct synthesis of imines through an oxidative process such as self-coupling of benzylamine has attracted much attention, owing to reduced energy consumption, and simplified procedures.[5,6] Furthermore, the utilization of solar light as the energy source for directly oxidizing benzylamine is a green and promising strategy.

For the oxidative coupling of benzylamine, CuCl was firstly used as the catalyst in the presence of air, and good activity was achieved.[7] Subsequently, many other catalysts for this reaction

have been explored. However, these catalytic reactions involve complex systems (oxidants and alkali auxiliaries), long reaction time, and are carried out at high temperatures and pressures.[8] Juntrapirom *et al.*[9] used O_2 as an oxidant to convert benzylamine with a conversion rate and selectivity of up to 94% and 85%, respectively, at room temperature and under visible light irradiation for 4 hours. This may be due to the fact that benzylamine reacts with pure oxygen to form a series of by-products. At a low reaction temperature (35 °C), Chai *et al.*[11] did not greatly improve the rate of benzylamine conversion carried out in air for 5 hours, although the selectivity was high (>99%). In the absence of O_2 and at a low reaction temperature (35 °C), Zhang *et al.*[10] achieved a conversion rate of 80% after conducting the reaction for a long time (200 hours). Therefore, it is still a challenge to increase the conversion of benzylamine under mild reaction conditions. It is well known that the pyrolysis of benzylamine releases toxic gases. Currently the most commonly used catalysts are expensive noble metals such as Ru,[12] Pd,[13] and Au.[14] Thus, researchers have turned their attention to cheaper catalysts containing non-noble metals such as g-C_3N_4,[15] Cu_2O,[16] Fe_2O_3,[17] and TiO_2,[18] which also show excellent photocatalytic performance.

Among them, g-C_3N_4 is an attractive organic semiconductor photocatalyst owing to its outstanding visible light activity, thermal and chemical stability. Interestingly, it can also be applied for the oxidative coupling of benzylamine under visible light.[19–21] Therefore, in this work, we present a $Cu/Cu_2O/Cu_3N$ ternary composite formed on C_3N_4 tubes for catalyzing the oxidative coupling reaction of benzylamine under visible-light

[a]*Key Laboratory of Functional Inorganic Material Chemistry, Ministry of Education of the People's Republic of China, School of Chemistry and Materials Science, Heilongjiang University, Harbin 150080, China. E-mail: jiangbaojiang88@sina.com; jbj@hlju.edu.cn*

[b]*Department of Chemistry and Biochemistry, Kent State University, Kent, OH 44242, USA. E-mail: Lzhang30@kent.edu*

[c]*Department of Food and Environment Engineering, Heilongjiang East University, Harbin, China. E-mail: 79652283@qq.com*

[d]*Institute of Chemistry, Saint Petersburg State University, Russia*

† Electronic supplementary information (ESI) available. See DOI: 10.1039/d0ra03164j

light using air as the oxidant. The conversion and selectivity of the reaction were as large as 99% and 98%, respectively. In particular, Cu_3N, which has shown prominent activity in the electrocatalytic hydrogen evolution and oxygen evolution reactions,[22,23] was explored for the first time as a co-photocatalyst for the coupling reaction.

2. Experimental

2.1 Materials

Copper acetate hydrate $(Cu(Ac)_2 \cdot H_2O$; analytically pure reagent, 99.98%), sodium hydroxide (NaOH; AR, 96%), melamine (AR, 99%) and dimethyl sulfoxide (DMSO; chromatographically pure, $\geq$99.8%) were purchased from Aladdin Reagent. Benzylamine (chromatographically pure, $\geq$99.0%) was bought from Sigma Aldrich. Deionized water was used during the experiments. The Cu_3N and Cu_2O used for testing and characterization in the experiment are purchased commercial products.

2.2 Fabrication of Cu_2O on a supramolecular precursor of C_3N_4

First, 5 mL of 0.8 M NaOH solution was slowly added into 30 mL of 0.1 M $Cu(Ac)_2$ solution under stirring for 20 min at 25 °C. Next, various amounts of melamine $[n_{Cu(Ac)2} : n_{melamine} = 1 : 1,$ $1 : 2, 1 : 3$ and $1 : 4$ (molar ratio)] were each added into the above solution, and the resultant suspensions were stirred in a water bath at 60 °C for 30 min. Subsequently, the mixture solutions were transferred into 50 mL polytetrafluoroethylene autoclaves and then kept at 180 °C for 10 h. Finally, black-brown precipitates were obtained by centrifugation, washed three times with hot water, and then dried at 60 °C for 6 h.

2.3 Fabrication of $Cu/Cu_2O/Cu_3N$ on hexagonal C_3N_4 tubes

The black-brown precipitates were each transferred to a porcelain boat and then were calcined at 400 °C for 2 h in an argon atmosphere that prevents the oxidation of Cu_2O (the flow rate was set at 5 mL min^{-1}). As a result, dark-green samples were obtained. These samples were named as $Cu/Cu_2O/Cu_3N/C_3N_4$-1, $Cu/Cu_2O/Cu_3N/C_3N_4$-2, $Cu/Cu_2O/Cu_3N/C_3N_4$-3, and $Cu/Cu_2O/$ Cu_3N/C_3N_4-4, corresponding to the molar ratio of $Cu(Ac)_2$ to melamine of $1 : 1$, $1 : 2$, $1 : 3$ and $1 : 4$, respectively.

2.4 Characterization

Morphologies of the samples were characterized through scanning electron microscopy (SEM) with Hitachi S-4800 operating at 15 KV and transmission electron microscopy (TEM) with JEMF200 an operating at an acceleration voltage of 200 kV. The X-ray diffraction (XRD) was conducted at room temperature on a Bruker D8 ADVANCE diffractometer with nickel-filtered Cu Ka radiation (λ = 1.5406 Å). X-ray photoelectron spectroscopy (XPS) was performed on VG ESCALAB MK II with an achromatic Mg Ka radiation (1253.6 eV) to analyze the electronic states of the surface. N_2 adsorption–desorption isotherms were recorded on Tristar II 3020 and surface areas were determined by using the Brunauer–Emmett–Teller (BET) method. UV-visible diffuse reflectance spectra (UV-vis DRS) were obtained on a Perkin-Elmer-Lambda 950 spectrophotometer using $BaSO_4$ as the referencing material. The photoluminescence (PL) spectra of the samples were measured with a spectrofluoro-photometer (Hitachi FLS1000) at an excitation wavelength of 375 nm. The Scanning Kelvin Probe (SKP) measurements (SKP5050 system, Scotland) were implemented under normal conditions (*i.e.*, room temperature and ambient pressure). Electrochemical impedance spectroscopy (EIS) measurements were performed under simulated sunlight irradiation at open circuit voltage over a frequency range from 105 to 0.05 Hz with an AC voltage of 5 mV. Mott–Schottky analysis was performed by using an electrochemical Princeton instrument at different frequencies *versus* the saturated Ag/AgCl electrode (pH = 7). Benzylamine and imine products were detected using GC-MS (Thermo Trace1300).

2.5 Photocatalytic oxidative coupling of benzylamine

To begin with, 40 mg of a prepared product was placed in a Schlenk flask. Subsequently, 3 mL of chromatographically pure dimethyl sulfoxide (DMSO) was added as the solvent, followed by 3 mmol of chromatographically pure benzylamine. Next, the flask was placed in a sonicator for 5 min until a homogeneous suspension was obtained. The suspension was then heated to 323 K using a heating mantle and irradiated with a 300 W Xe lamp for 12 h. After the reaction, 1 mL of the suspension was taken and passed through a 0.22 μm organic filter to remove the catalyst. The resulting filtrate was extracted with ethyl acetate and then analyzed by GC-MS.

3. Results and discussion

3.1 Crystal structure and morphology

As is evident from the SEM image (Fig. 1a), the assembly of melamine in the presence of NaOH resulted in a supramolecular precursor of C_3N_4 with a hexagonal rod-like structure, and the rods are evenly decorated with a large number of CuO particles generated from the reaction between copper acetate and the base. Interestingly, after calcination these solid rods became smaller and hollow, producing a tubular structure (Fig. 1b and c). Moreover, the particles on the surface of each tube aggregated. In the high-resolution TEM (HRTEM) image of the calcined product, two lattice fringes can be clearly seen (Fig. 1d), which correspond to the (111) crystal plane of Cu_2O (d_{111} = 0.24 nm) and the (111) crystal plane of Cu_3N (d_{111} = 0.22 nm), respectively. In other words, copper(II) oxide was reduced to highly crystalline copper(I)-containing species during the thermal treatment. The presence of C, N, Cu, and O was verified by elemental mapping and these elements are uniformly distributed across the tubular structure (Fig. 1e–h).

Phases of the product were further investigated by XRD experiments. It turned out that samples synthesized from different Cu $(Ac)_2$/melamine molar ratios have similar patterns (Fig. 2a). The peaks at 43.2°, 50.4° and 74.1° correspond to the (111), (200) and (220) crystal planes of Cu (PDF# 04-0836); those at 36.4°, 42.2° and 61.3° can be indexed to the (111), (200) and (220) crystal planes of Cu_2O (PDF# 05-0667); lastly, the peaks at
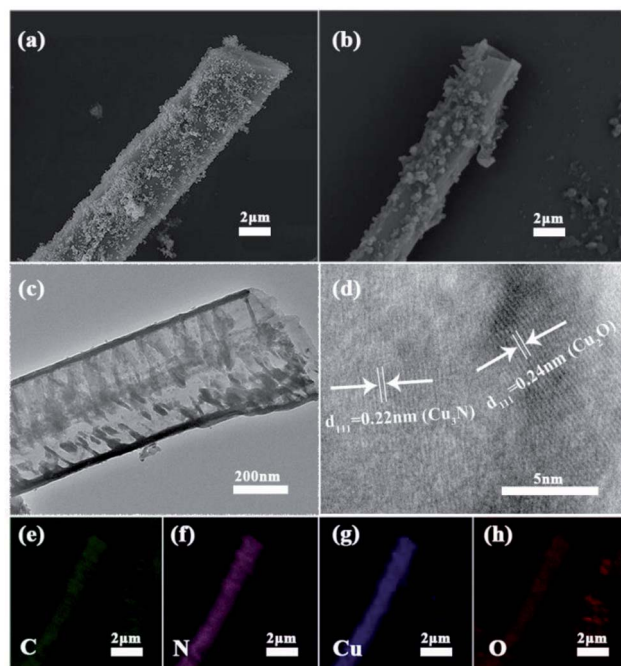
Fig. 1 High-magnification SEM images of (a) the precursor and (b) Cu/Cu$_2$O/Cu$_3$N/C$_3$N$_4$-3; (c) TEM and (d) HRTEM images of Cu/Cu$_2$O/Cu$_3$N/C$_3$N$_4$-3; (e–h) elemental mappings of C, N, Cu, O for Cu/Cu$_2$O/Cu$_3$N/C$_3$N$_4$-3 in the region shown in (b).

23.2°, 40.8° and 47.5° correspond to the (100), (111) and (200) crystal planes of Cu$_3$N (PDF# 47-1088).[24–29] Further, a weak broad peak at about 27° is visible, which is attributable to the X-ray reflections from the (002) crystal planes of C$_3$N$_4$ (corresponding to interlayer stacking).[30,31] Moreover, all these characteristic peaks are sharp and strong due to the good crystallinity of Cu, Cu$_2$O, and Cu$_3$N, which is in line with the TEM result. However, the crystallinity of carbon nitride is poor. Although the diffraction of X-rays by C$_3$N$_4$ is not well resolved due to the presence of Cu$_2$O with higher crystallinity (Fig. 2a and S1†), in the XRD pattern of pure C$_3$N$_4$ synthesized without copper acetate pure, the characteristic peaks at 13° and 27° can be clearly seen (Fig. S2†), verifying that C$_3$N$_4$ indeed can be synthesized by the thermal polymerization of melamine. As the Cu(Ac)$_2$/melamine molar ratio was increased, the content of C$_3$N$_4$ increases, the crystallinity of the composite will also decrease, as a result, Cu XRD peaks became weaker, indicating a decrease in the Cu content. This result was further verified by inductively coupled plasma (ICP) measurements, which show that the mass percentage was reduced from 66.46% (Cu/Cu$_2$O/Cu$_3$N/C$_3$N$_4$-1) to 33.47% (Cu/Cu$_2$O/Cu$_3$N/C$_3$N$_4$-4, Table S1†). In the FT-IR spectrum (Fig. S3†), the peak at 808 cm^{-1} is attributable to the vibration of the triazine ring, further supporting the presence of CN in Cu/Cu$_2$O/Cu$_3$N/C$_3$N$_4$. As the amount of melamine increases, the vibration intensity of C$_3$N$_4$ also strengthens. The peaks appearing in the range of 1200–1600 cm^{-1} are due to the tensile vibration of C–N and C=N. The broad peak in the range of 3100–3300 cm^{-1} is formed by the
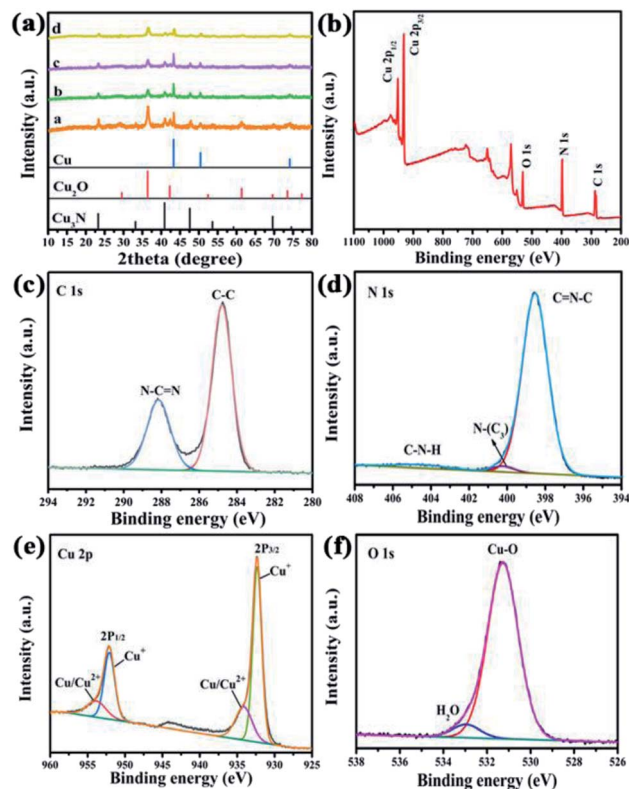

Fig. 2 (a) XRD patterns. (a) Cu/Cu$_2$O/Cu$_3$N/C$_3$N$_4$-1; (b) Cu/Cu$_2$O/Cu$_3$N/C$_3$N$_4$-2; (c) Cu/Cu$_2$O/Cu$_3$N/C$_3$N$_4$-3; (d) Cu/Cu$_2$O/Cu$_3$N/C$_3$N$_4$-4. (b) XPS survey spectrum of Cu/Cu$_2$O/Cu$_3$N/C$_3$N$_4$-3; high-resolution XPS (c) C 1s, (d) N 1s, (e) Cu 2p, and (f) O 1s spectra of Cu/Cu$_2$O/Cu$_3$N/C$_3$N$_4$-3.

stretching vibration of N–H and O–H owing to adsorbed water molecules.

The chemical state of the synthesized materials and the elemental composition on the surfaces were studied by X-ray photoelectron spectroscopy (XPS). The characteristic peaks of C, N, Cu, and O are clearly visible in the survey spectrum (Fig. 2b), suggesting that the surface regions of the materials contain the same elements as the bulk parts. The high-resolution XPS C 1s spectrum exhibits two peaks at 284.6 eV and 288.1 eV (Fig. 2c), which can be assigned to carbon in C–C and N–C=N (namely sp^2-hybridized C), respectively.[32,33] The XPS N 1s spectrum can be deconvoluted into two core lines, featuring three peaks (Fig. 2d). The peak at 398.5 eV corresponds to N of the triazine ring (C=N–C) or Cu–N, and the peak at 400.2 eV is due to surface-adsorbed NH$_3$ (which was produced during the thermal polymerization of melamine) and tertiary nitrogen in the N–(C)$_3$ or HN(C)$_2$ groups. The peak at 404.5 eV belongs to C–N–H.[34,35] Therefore, the XPS results verify the successful preparation of C$_3$N$_4$.

In the XPS Cu 2p spectrum (Fig. 2e), a pair of peaks at 932.7 eV and 953.7 eV can be ascribed to 2p$_{3/2}$ and 2p$_{1/2}$, respectively, of Cu$^+$.[36] Another pair of peaks at 934.2 eV and 954.6 eV are attributed to metallic Cu^0 or Cu^{2+}.[37] According to XRD characterization, there are characteristic peaks of Cu and no characteristic peaks of Cu^{2+} are found. Therefore, these two

peaks are Cu, while the peak of Cu$^+$ belongs to Cu$_2$O in the catalyst. Hence, XPS further confirms the XRD result that during the thermal treatment of the supramolecular precursor CuO can be reduced to Cu and Cu$_2$O, possibly due to the reducing gases such as NH$_3$ released. The presence of two types of oxygen, namely lattice oxygen and oxygen in the water adsorbed on the surface, is evidenced by the peaks at 531.3 eV, and 532.9 eV, respectively, in the XPS O 1s spectrum (Fig. 2f).[38] Quantitative analysis by using elemental analysis revealed that the C/N ratio for all the composites (Table S2†) is smaller than the theoretical value for C$_3$N$_4$ (*i.e.*, 0.6428).[39] Particularly, Cu/Cu$_2$O/Cu$_3$N/C$_3$N$_4$-3 has the smallest C/N ratio (0.5767). Carbon nitride with a larger percentage of N is believed to have more active sites and therefore give better photocatalytic performance. Hence, Cu/Cu$_2$O/Cu$_3$N/C$_3$N$_4$-3 was selected for the remaining experiments.

3.2 Optical properties and charge dynamics

Fig. 3a and S4a† show the diffuse reflectance spectra (DRS) of Cu$_2$O, Cu$_3$N, C$_3$N$_4$ and Cu/Cu$_2$O/Cu$_3$N/C$_3$N$_4$-3 in the 300–900 nm range. The absorption spectrum of Cu/Cu$_2$O/Cu$_3$N/C$_3$N$_4$-3 is similar to that of Cu$_3$N but is slightly shifted toward larger absorbance. Cu$_3$N, Cu$_2$O and Cu/Cu$_2$O/Cu$_3$N/C$_3$N$_4$-3 show stronger optical absorption than C$_3$N$_4$ at wavelengths above the absorption edge of C$_3$N$_4$, namely 579.9 nm. The optical band gaps of Cu$_2$O, Cu$_3$N, C$_3$N$_4$ and Cu/Cu$_2$O/Cu$_3$N/C$_3$N$_4$-3 were determined to be 1.89 eV, 1.12 eV, 2.19 eV and 0.82 eV, respectively, from the Tauc plots displayed in Fig. 3b and S4b.†
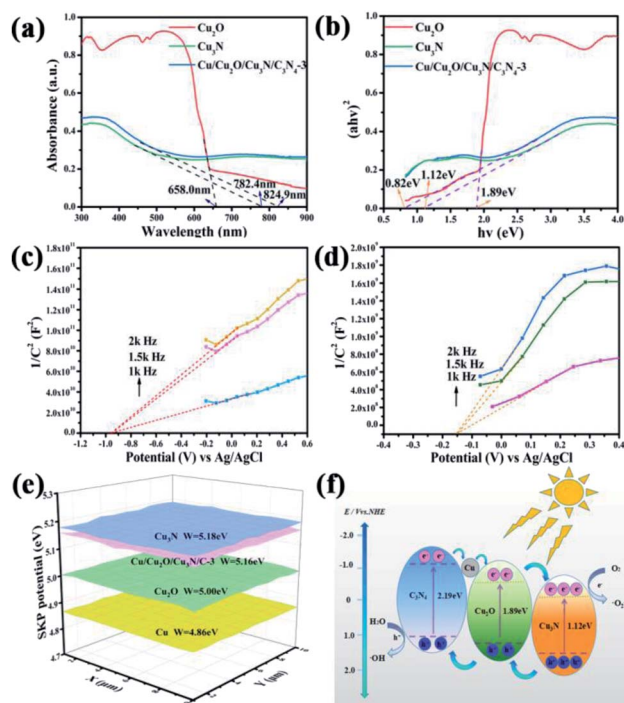
Photocatalysts with small band gaps are more favorable owing to their enhanced light absorption ability.

Mott–Schottky plots of Cu$_3$N and Cu$_2$O at three frequencies (*i.e.*, 1.0 kHz, 1.5 kHz, and 2.0 kHz) were recorded to determine the flat-band potentials. The flat-band potentials of Cu$_3$N, Cu$_2$O and C$_3$N$_4$ were assessed to be about 0.04, −0.76 and −1.12 (*vs.* NHE), respectively, by extrapolation. In turn, the valence band edges of Cu$_3$N, Cu$_2$O and C$_3$N$_4$ were calculated by using the band gaps. Based on the potential difference, electrons in Cu$_3$N transfer to Cu$_2$O. To further confirm this electron transfer direction, scanning Kelvin probe (SKP) was utilized to determine the work functions, which were calculated according to the following formula: $W = 5.1 + W_{ave}/1000$, where W and W_{ave} refer to the work function and work function average, respectively. It turned out that the work function decreases in the order of Cu$_3$N > Cu/Cu$_2$O/Cu$_3$N/C$_3$N$_4$-3 > Cu$_2$O > Cu (Fig. 3e). In other words, the Fermi level relative to the vacuum level increases in the order Cu$_3$N < Cu/Cu$_2$O/Cu$_3$N/C$_3$N$_4$-3 < Cu$_2$O < Cu; therefore, in the Cu/Cu$_2$O/Cu$_3$N/C$_3$N$_4$-3 heterojunction electrons transfer from Cu to Cu$_2$O and finally to Cu$_3$N. The band diagram of Cu/Cu$_2$O/Cu$_3$N/C$_3$N$_4$-3 is shown in Fig. 3f and S5.† Under the irradiation of visible light, Cu$_2$O, Cu$_3$N, and C$_3$N$_4$ are excited and electron–hole pairs are generated. According to the potential difference, the electrons on C$_3$N$_4$ are transferred to Cu, then to Cu$_2$O and finally to Cu$_3$N. In the meanwhile, holes are transferred from Cu$_3$N to Cu$_2$O and finally transported to C$_3$N$_4$. Subsequently, electrons react with O$_2$ and holes react with water to produce highly reactive ·O$_2^-$ and ·OH, respectively, which may induce the coupling reaction of benzylamine. The specific surface area (SSA) and pore size of Cu/Cu$_2$O/Cu$_3$N/C$_3$N$_4$-3 were determined to be 45.6 m^2 g^{-1} and 24.0 nm, respectively, from nitrogen adsorption–desorption isotherms (Fig. S5†). SSA of Cu/Cu$_2$O/Cu$_3$N/C$_3$N$_4$-3 is larger than those of Cu, Cu$_2$O, and Cu$_3$N, indicating that the former has the most reaction sites on its surface, which is beneficial to the oxidation of benzylamine.

The performance of a photocatalyst greatly depends on its charge dynamics, which can be investigated by photoluminescence (PL) spectroscopy and electrochemical impedance spectroscopy (EIS).[40] The measurement of PL intensity for different samples at an excitation wavelength of 375 nm is shown in Fig. 4a. As can be seen, the PL intensity of Cu/Cu$_2$O/Cu$_3$N/C$_3$N$_4$-3 is much lower than that of other samples, illustrating that the recombination of the electron–hole pairs in Cu/
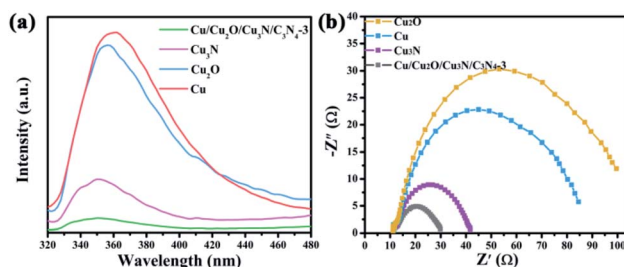

Fig. 3 (a) Diffuse reflectance spectra (DRS) and (b) Tauc plots of Cu$_2$O, Cu$_3$N and Cu/Cu$_2$O/Cu$_3$N/C$_3$N$_4$-3. (c) Mott–Schottky plots of Cu$_2$O and (d) Cu$_3$N at various frequencies (pH = 7). (e) Scanning Kelvin probe mappings (SKP) of Cu$_2$O, Cu$_3$N and Cu/Cu$_2$O/Cu$_3$N/C$_3$N$_4$-3. (f) Energy band diagram.

Fig. 4 (a) Photoluminescence spectra of Cu, Cu$_2$O, Cu$_3$N and Cu/Cu$_2$O/Cu$_3$N/C$_3$N$_4$-3. (b) Nyquist plots of Cu, Cu$_2$O, Cu$_3$N and Cu/Cu$_2$O/Cu$_3$N/C$_3$N$_4$-3.

$Cu_2O/Cu_3N/C_3N_4$-3 is suppressed as compared with other samples. The conclusion is further confirmed by EIS (Fig. 4b). The Nyquist plot of $Cu/Cu_2O/Cu_3N/C_3N_4$-3 displays the smallest semicircle among all samples studied, which indicates that it has the smallest interfacial charge transfer resistance.

3.3 Photocatalytic tests

Photocatalysis is typically conducted at mild and environmentally friendly conditions, and it involves the generation of electrons and holes that trigger a series of redox reactions.[41] The performance of the synthesized materials toward photocatalytic coupling reaction of benzylamine in the presence of air and at 323 K is shown in Table 1. It can be seen that both Cu_2O and Cu_3N are able to induce the oxidative coupling reaction of benzylamine and the conversion was 12% and 80%, respectively. However, $Cu/Cu_2O/Cu_3N/C_3N_4$ photocatalysts exhibited higher activities. Although Cu_3N plays a major role in the reaction, Cu_2O and Cu can catalyze the oxidation of benzylamine and thereby promote the reaction. Additionally, it was observed that for $Cu/Cu_2O/Cu_3N/C_3N_4$-3 the selectivity and conversion of benzylamine oxidation were 98% and 99%, respectively. In order to further study the effect of light on the catalytic reaction, a benzylamine oxidative coupling reaction was performed under a single reaction condition only, and the results are included in Table S3.† When $Cu/Cu_2O/Cu_3N/C_3N_4$-3 was heated to 50 °C (323 K) without light, the conversion and selectivity were very low, reaching only 33% and 94%, respectively. After light was introduced, the conversion and selectivity were increased to 74% and 98%, respectively. The results of oxidative coupling of benzylamine in different atmospheres are listed in Table S4.† It was found that under inert gas, the conversion rate of benzylamine is very low, only 44%, but the selectivity reaches 98%. In an atmosphere containing oxygen, the conversion of benzylamine can be close to 100%, but the selectivity of benzylamine under pure oxygen is lower than that under air. This may be due to the reaction of benzylamine with oxygen that produces some by-products such as benzylalcohol

and benzaldehyde. All the above data are derived from Gas Chromatography-Mass Spectrometer (GC-MS). This paper uses external standard method to fit the line graph of benzylamine concentration and peak area as shown in the Fig. S6.† The benzylamine peak area acquired by the GC-MS test was calculated by a one-time function formula (Fig. S6†) to obtain the benzylamine concentration, and the benzylamine conversion rate was calculated. With reasonable test conditions, the retention time of chromatographic grade benzylamine is 1.69 min, as shown in the Fig. S7.†

The photocatalytic activity of $Cu/Cu_2O/Cu_3N/C_3N_4$-3 was further studied by using many benzylamine derivatives with electron withdrawing or donating groups as the substrates. The electron-withdrawing groups include –F, –Cl, –Br, $–OCH_3$ and $–CF_3$, while the electron-donating groups include $–CH_3$ and $–(CH_3)_3C$. The conversion rates involving the electron-donating groups are 98% for 4-methylbenzylamine and 78% for 4-*tert*-butylbenzylamine, while those involving the electron-withdrawing groups are 89% (–F), 85% (–Cl), 82% (–Br), 72% ($–CF_3$) and 88% ($–OCH_3$). Generally, electron-donating groups have stronger oxidizing ability than electron-withdrawing groups;[42] however, it is not clearly reflected in the present work. Interestingly, the conversion rate of 4-*tert*-butylbenzylamine coupling was 20% lower than that of 4-methylbenzylamine coupling, indicating that the *tert*-butyl group is not conducive to the photocatalytic benzylamine coupling reaction, which may be ascribed to the steric effect.[43] Furthermore, both the conversion and selectivity for the coupling reaction of any benzylamine with a methyl group were larger than 90% regardless of the position of the group. From the table, it finds that the conversion and selectivity of benzylamine with different groups are at the upper levels, indicating that the catalyst has a promoting effect on the organic reaction (Table 2).

3.4 Mechanism of photocatalytic benzylamine coupling

The underlying mechanism of the coupling reaction of benzylamines was studied by electron spin resonance (ESR). To detect $\cdot OH$ and $\cdot O_2^-$, 5, 5-dimethyl-1-pyrroline-*N*-oxide (DMPO) that captures these radicals was added. Based on the ESR spectra shown in Fig. 5a and b, the amount of these two radicals decreases in the sequence of $Cu/Cu_2O/Cu_3N/C_3N_4$-3 > Cu_3N > Cu > Cu_2O, which is consistent with their oxidation performance discussed above. $\cdot O_2^-$ has a stronger oxidizing ability than $\cdot OH$, and therefore plays a major role in the photocatalytic coupling of benzylamine. Samples for GC-MS were taken at 3rd, 6th, 9th and 12th hour during the oxidative coupling reaction of benzylamine. The mass spectrum of the 3rd-hour sample shows peaks at m/z = 103, 105, 106.12, 107.15 and 108.13, corresponding to benzonitrile, intermediate I, benzaldehyde, benzylamine and benzylalcohol, respectively (Fig. S8a†). At the same time, a peak at m/z = 194.15, which belongs to imine, can be observed in the mass spectrum of the 3rd-hour sample (Fig. S8b†). In the chromatogram (Fig. S8c–f†), peaks with retention times of 1.69 and 1.71 are the characteristic peaks of benzylamine, while peaks with retention times of 5.41 and 5.42 belong to imines. As benzylamine was consumed while the

Table 1 Coupling reaction of benzylamine with different catalysts[a]

Sample	Conversion	Selectivity
Cu_2O	12%	99%
Cu	77%	89%
Cu_3N	80%	85%
$Cu/Cu_2O/Cu_3N/C_3N_4$-1	93%	96%
$Cu/Cu_2O/Cu_3N/C_3N_4$-2	97%	92%
$Cu/Cu_2O/Cu_3N/C_3N_4$-3	99%	98%
$Cu/Cu_2O/Cu_3N/C_3N_4$-4	60%	98%
—	7%	62%

[a] Reaction condition: 3 mmol benzylamine, 12 h, 40 mg $Cu/Cu_2O/Cu_3N/C_3N_4$-3, cut 420 nm with 300 mW cm^{-2}, Xe lamp, 3 mL dimethyl sulfoxide (DMSO), 323 K and air atmosphere.

Table 2 Selective oxidation of different aromatic amines with Cu/Cu$_2$O/Cu$_3$N/C$_3$N$_4$-3 as the catalyst[a]

Substrate	Produce	Con.	Sel.
benzylamine (C$_6$H$_5$CH$_2$NH$_2$)	N-benzylidene-benzylamine imine	99%	98%
4-F benzylamine	4,4'-difluoro imine	89%	98%
4-Cl benzylamine	4,4'-dichloro imine	85%	96%
4-Br benzylamine	4,4'-dibromo imine	82%	96%
4-CF$_3$ benzylamine	4,4'-bis(CF$_3$) imine	72%	97%
4-OCH$_3$ benzylamine	4,4'-dimethoxy imine	88%	98%
4-tert-butyl benzylamine	4,4'-di-tert-butyl imine	78%	94%
2-CH$_3$ benzylamine	2,2'-dimethyl imine	96%	92%
3-CH$_3$ benzylamine	3,3'-dimethyl imine	98%	95%
4-CH$_3$ benzylamine	4,4'-dimethyl imine	98%	96%
cyclohexylmethanamine	cyclohexyl imine	92%	95%

[a] Reaction condition: 3 mmol different aromatic amines, 12 h, 40 mg Cu/Cu$_2$O/Cu$_3$N/C$_3$N$_4$-3, cut 420 nm with 300 mW cm^{-2}, Xe lamp, 3 mL dimethyl sulfoxide (DMSO) and air atmosphere.
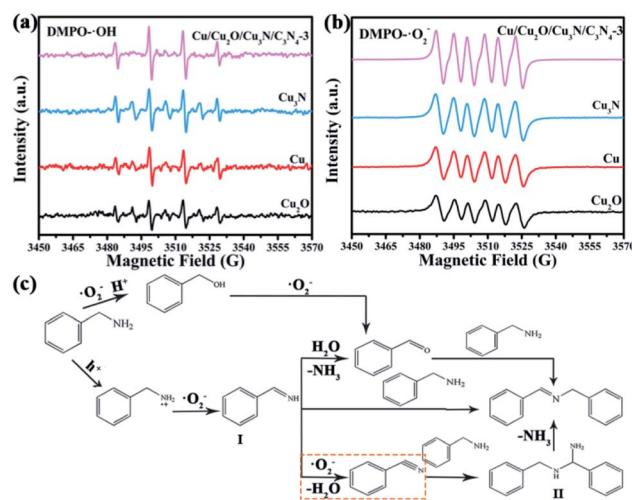

Fig. 5 Electron spin resonance (ESR) spectra of radicals trapped by 5,5-dimethyl-1-pyrroline-N-oxide (DMPO) in (a) aqueous dispersion for DMPO-·OH and (b) methanol dispersion for DMPO-·O$_2^-$. (c) Proposed processes toward the formation of an imine from benzylamine over Cu/Cu$_2$O/Cu$_3$N/C$_3$N$_4$-3.

imine was produced, the relative intensity of the imine peak to the benzylamine peak was increased. And it is also accompanied by the conversion of some by-products to imine.

Therefore, two possible oxidation pathways are proposed in Fig. 5c. The first pathway is a traditional synthesis method, namely oxidative condensation of benzylalcohol and benzylamine to obtain imine. In the first pathway, benzylamine is oxidized by ·O$_2^-$ to benzylalcohol with $m/z = 108.13$ and then to benzaldehyde with $m/z = 106.12$, which is subsequently dehydrated and condensed with a benzylamine molecule through nucleophilic substitution, producing an imine with $m/z = 194.15$. Specifically, the O atom bonded with α-C is replaced by the N atom of –NH$_2$ in a benzylamine molecule.[44]

In the second pathway, a benzylamine molecule becomes a positively charged benzylamine radical with the help of a hole and then the benzylamine radical is oxidized by ·O$_2^-$ to form an imine intermediate I with $m/z = 105$,[45] which is converted to

imine through three ways. The first way is the hydrolysis of intermediate I that releases NH$_3$ molecules and creates benzaldehyde with $m/z = 106.12$.[46] Same as the last step of the first pathway, the reaction between benzaldehyde and benzylamine results in the imine with the release of H$_2$O.[47] Also, a simpler and more dominant way is that intermediate I directly reacts with benzylamine and imine is produced as one of the two products (NH$_3$ being the other product).[48] The last way starts with the dehydration of intermediate I with the help of ·O$_2^-$, which yields benzonitrile ($m/z = 103$).[49] Next, benzonitrile reacts with benzylamine to form a diamine (intermediate II), which then undergoes deamination to give an imine. This third path mainly occurs as a side reaction.[49]

4. Conclusions

In summary, ternary Cu/Cu$_2$O/Cu$_3$N heterostructures have been successfully prepared on C$_3$N$_4$ tubes by hydrothermal synthesis and heat treatment. Cu and Cu$_3$N in the composites protect Cu$_2$O from photo-corrosion and improve the photocatalytic activity. Particularly, Cu/Cu$_2$O/Cu$_3$N/C$_3$N$_4$-3 is responsive to a wide range of light from visible to near-infrared, and is able to produce highly reactive ·O$_2^-$. Therefore, under visible light irradiation, Cu/Cu$_2$O/Cu$_3$N/C$_3$N$_4$-3 can induce the synthesis of imine at 323 K by using benzylamine. The conversion and selectivity of benzylamine coupling reaction are up to 99% and 98%, respectively. This work not only demonstrates the potential of Cu$_3$N and other copper-based semiconductors for organic synthesis, but also presents a promising strategy involving photocatalysis towards imine production through the coupling reaction of benzylamine.

Conflicts of interest

There are no conflicts to declare.

Acknowledgements

Notes and references

1 H. X. Wei, Z. F. Guo, X. Liang, P. Q. Chen, H. Liu and H. Z. Xing, *ACS Appl. Mater. Interfaces*, 2019, **11**, 3016–3023.

2 J. I. Yang and C. Y. Mou, *Appl. Catal., B*, 2018, **231**, 283–291.

3 H. Naeimi, F. Salimi and K. Rabiei, *J. Mol. Catal. A: Chem.*, 2006, **260**, 100–104.

4 J. N. Young, T. C. Chang, S. C. Tsai, L. Yang and S. C. Yu, *J. Catal.*, 2010, **272**, 253.

5 S. Furukawa, Y. Ohno, T. Shishido, K. Teramura and T. Tanaka, *ACS Catal.*, 2011, **1**, 1150.

6 M. H. So, Y. G. Liu, C. M. Ho and C. M. Che, *Chem.–Asian J.*, 2009, **4**, 1551.

7 R. D. Patil and S. Adimurthya, *Adv. Synth. Catal.*, 2011, **353**, 1695–1700.

8 J. M. Bermudez, J. A. Menendez, A. Arenillas, R. M. Palou, A. A. Romero and R. Luque, *J. Mol. Catal. A: Chem.*, 2015, **406**, 19–22.

9 S. Juntrapirom, S. Anuchai, O. Thongsook, S. Pornsuwan, P. Meepowpan, P. Thavornyutikarn, S. Phanichphant, D. Tantraviwat and B. Inceesungvorn, *Chem. Eng. J.*, 2020, **394**, 124934.

10 Y. W. Zhang, J. S. Xu, J. Mei, S. Sarina, Z. Y. Wu, T. Liao, C. Yan and Z. Q. Sun, *J. Hazard. Mater.*, 2020, **394**, 122529.

11 Y. Y. Chai, L. Zhang, Q. Q. Liu, F. l. Yang and W. L. Dai, *ACS Sustainable Chem. Eng.*, 2018, **6**, 10526–10535.

12 K. Yamaguchi and N. Mizuno, *Angew. Chem., Int. Ed.*, 2003, **42**, 1480–1483.

13 R. S. Wang, G. H. Qiu, Y. Xiao, X. Q. Tao, W. Peng and B. X. Li, *J. Catal.*, 2019, **374**, 378–390.

14 Z. X. Qin, D. Zhao, L. Zhao, Q. Xiao, T. T. Wu, J. W. Zhang, C. Q. Wan and G. Li, *Nanoscale Adv.*, 2019, **1**, 2529.

15 K. X. Zhang, H. Su, H. H. Wang, J. J. Zhang, S. Y. Zhao, W. W. Lei, X. Wei, X. H. Li and J. S. Chen, *Adv. Sci.*, 2018, **5**, 1800062.

16 M. Gopiraman and I. M. Chung, *J. Taiwan Inst. Chem. Eng.*, 2017, **81**, 455–464.

17 R. Mazzaro, S. B. Bibi, M. Natali, G. Bergamini, V. Morandi, P. Ceroni and A. Vomiero, *Nano Energy*, 2019, **61**, 36–46.

18 T. Yang, Q. M. Yu and H. M. Wang, *Catal. Lett.*, 2018, **148**, 2382–2390.

19 X. C. Wang, K. Maeda, A. Thomas, K. Takanabe, G. Xin, J. M. Carlsson, K. Domen and M. Antonietti, *Nat. Mater.*, 2009, **8**, 76–80.

20 J. Liu, Y. Liu, N. Y. Liu, Y. Z. Han, X. Zhang, H. Huang, Y. Lifshitz, S. T. Lee, J. Zhong and Z. H. Kang, *Science*, 2015, **347**, 970–974.

21 S. E. Guo, Z. P. Deng, M. X. Li, B. J. Jiang, C. G. Tian, Q. J. Pan and H. G. Fu, *Energy Environ. Sci.*, 2011, **4**, 2922–2929.

22 C. Panda, P. W. Menezes, M. Zheng, S. Orthmann and M. Driess, *ACS Energy Lett.*, 2019, **4**, 747–754.

23 H. L. Liu, Q. Wu, L. M. Li and X. S. Tai, *Dalton Trans.*, 2019, **16**, 5131–5134.

24 Y. M. Juan, S. J. Chang, H. T. Hsueh, S. H. Wang, T. C. Cheng, S. W. Huang and C. L. Hsu, *RSC Adv.*, 2015, **67**, 54220–54224.

25 F. L. Meng, H. X. Zhong, Q. Zhang, K. H. Liu, J. M. Yan and Q. Jiang, *J. Mater. Chem. A*, 2017, **5**, 18972.

26 Z. P. Zeng, Y. B. Yan, J. Chen, P. Zan, Q. H. Tian and P. Chen, *Adv. Funct. Mater.*, 2018, **29**, 1806500.

27 S. R. Ye, A. R. Rathmell, A. R. Wilson and B. J. Wiley, *Small*, 2014, **10**, 1771–1778.

28 C. Y. Su, B. H. Liu, T. J. Lin, Y. M. Chi, C. C. Kei, K. W. Wang and T. P. Perng, *J. Mater. Chem. A*, 2015, **3**, 18983.

29 F. L. Meng, H. X. Zhong, Q. Zhang, K. H. Liu, J. M. Yan and Q. Jiang, *J. Mater. Chem. A*, 2017, **5**, 18972.

30 J. S. Zhang, X. F. Chen, K. Takanabe, K. Maeda, K. Domen, J. D. Epping, X. Z. Fu, M. Antonietti and X. C. Wang, *Angew. Chem., Int. Ed.*, 2010, **49**, 441–444.

31 S. E. Guo, Y. Q. Tang, Y. Xie, C. G. Tian, Q. M. Feng, W. Zhou and B. J. Jiang, *Appl. Catal., B*, 2017, **218**, 664–671.

32 J. Zhang, M. Zhang, G. Zhang and X. Wang, *ACS Catal.*, 2012, **2**, 940–944.

33 F. Dong, Z. W. Zhao, T. Xiong, Z. L. Ni, W. D. Zhang, Y. J. Sun and W. K. Ho, *Appl. Mater. Interfaces*, 2013, **5**, 11392–11401.

34 R. Deshmukh, G. B. Zeng, E. Tervoort, M. Staniuk, D. Wood and M. Niederberger, *Chem. Mater.*, 2015, **27**, 8282–8288.

35 F. Hou, Y. Li, Y. T. Gao, S. Hu, B. G. Wu, H. L. Bao, H. Wang and J. B. Jiang, *Mater. Res. Bull.*, 2019, **110**, 18–23.

36 J. Zhang, J. G. Yu, Y. M. Zhang, Q. Li and J. R. Gong, *Nano Lett.*, 2011, **11**, 4774–4779.

37 S. Zhang, X. Wen, M. Long, J. Xi, J. Hu and A. Tang, *J. Alloys Compd.*, 2020, **829**, 154568.

38 A. Mitra, P. Howli, D. Sen, B. Das and K. K. Chattopadhyay, *Nanoscale*, 2016, **8**, 19099–19109.

39 Y. Q. Tang, M. Yuan, B. J. Jiang, Y. T. Xiao, Y. Fu, S. Chen, Z. P. Deng, Q. J. Pan, C. G. Tian and H. G. Fu, *J. Mater. Chem. A*, 2017, **5**, 21979–21985.

40 P. Z. Qiao, B. J. Sun, H. Z. Li, Y. C. Xu, L. P. Ren, K. Pan, L. Wang and W. Zhou, *ACS Appl. Mater. Interfaces*, 2019, **11**, 7066–7073.

41 M. Mousavi, A. H. Yangjeh and S. R. Pouran, *J. Mater. Sci.: Mater. Electron.*, 2018, **29**, 1719–1747.

42 S. Furuawa, Y. Ohno, T. Shishido, K. Teramura and T. Tanaka, *ACS Catal.*, 2011, **1**, 1150–1153.

43 A. L. Yuan, H. Lei, Z. S. Wang and X. P. Dong, *J. Colloid Interface Sci.*, 2020, **560**, 40–49.

44 P. Bai, X. l. Tong, J. Wan, Y. Q. Gao and S. Xue, *J. Catal.*, 2019, **374**, 257–265.

45 G. H. Qiu, R. S. Wang, F. Han, X. Q. Tao, Y. Xiao and B. X. Li, *Ind. Eng. Chem. Res.*, 2019, **58**, 17389–17398.

46 Y. Xiao, X. Q. Tao, G. H. Qiu, Z. F. Dai, P. Gao and B. X. Li, *J. Colloid Interface Sci.*, 2019, **550**, 99–109.

47 M. Largeron and M. B. Fleury, *Chem.–Eur. J.*, 2015, **21**, 1.

48 T. Wang, X. Q. Tao, Y. Xiao, G. H. Qiu, Y. Yang and B. X. Li, *Catal. Sci. Technol.*, 2020, **10**, 138–146.

49 M. M. Wang, H. H. Wu, C. R. Shen, S. P. Luo, D. Wang and L. He, *ChemCatChem*, 2019, **11**, 1935–1942.